Journal of Power, Energy, and Control

Research article

Fault Detection in Grid-Connected Photovoltaic Systems Using Extended State Estimation and Residual Analysis

Yaouba[1,2,*], Albert Ayang[1], Ahmat Tom[3], Yacoub Nassian Nimir[1], Noël Djongyang[1]

[1]Department of Renewable Energy, National Advance School of Engineering of Maroua, University of Maroua, Cameroon

[2]Renewable Energies Research Center, Institute of Geological and Mining Research, Yaoundé, Cameroon

[3]Department of Energy Engineering, University Institute of Technology, University of Ngaoundéré, Cameroon

*Correspondence: yaoubadams21@gmail.com

https://doi.org/10.62777/pec.v3i1.110

Received: 13 December 2025
Revised: 9 May 2026
Accepted: 14 May 2026
Published: 26 May 2026

Abstract: This paper presents an approach to detect faults in Photovoltaic (PV) systems based on a state estimation and residual analysis. After constructing the mathematical model of the nonlinear system and the extended state observer, we establish the fault detection method of the Single-Phase Grid connected PV system subjected to external disturbances based on estimation and residual analysis of nominal and extended states. To manage the uncertainties due to the modeling and external disturbances, an active disturbance rejection control (ADRC) is used, thanks to its robustness. We generated residuals by comparing the actual and estimated states with a threshold set at a tolerance of 5% from the nominal residual value. The external disturbances, such as PV generator and grid voltage variations, are defined as the external sources of disturbances. The faults occasioned by these disturbances are detected by the presence of peaks exceeding the thresholds. The results obtained by simulation in MATLAB environment demonstrated that with a threshold set at a tolerance of 5% from the nominal residual value, the proposed residual analysis method achieves 62.5 % of detection of faults from the PV source and 100% detection of faults from the grid side. The state estimation-based approach is verified by a direct visual observation of the nominal (current and voltage) and extended (disturbances) state estimation curves. Given the satisfactory results of this work, this diagnosis approach offers an interesting outlook for ensuring the productivity and lifespan of the PV system.

Keywords: Photovoltaic systems, fault detection, state estimation, residual analysis, extended state observer, active disturbance rejection control.

1. Introduction

Due to growing populations, industrial development, and environmental concerns about global warming, renewable energy sources have emerged as an answer to the high demand for clean and sustainable energy [1]. Electricity generation from solar photovoltaic energy has attracted considerable interest worldwide. Due to the huge

potential for solar irradiation in the world in general and in Africa in particular, Photovoltaic technology has seen a great deal of installation capacity over the years [2]. The fluctuation of the PV energy source voltage and grid voltage, and the change in system parameters, lead to the instability of the output voltage [3]. For a dynamic system, accuracy, speed, and stability are very important parameters. However, disturbances, non-linearities, and uncertainties are real obstacles in this process [4]. It is essential to develop effective, accurate, and reliable methods and tools for the rapid detection of potential faults in order to optimize production and minimize the maintenance costs of photovoltaic installations [5]. Fault detection consists of making a binary decision whether or not a fault has occurred, while identification determines the location of the faulty component [6].

Some authors categorize faults in a PV system as either hard or soft. Blown fuses, damaged cables, or disconnection causes hard failures from the electrical grid due to inverter failure. Soft failures are caused by dust and dirt deposits on the panels' surface, hot spots, or partial shading [5]. Hard failures in the PV system generally lead to a drastic and rapid variation in electrical variables. Thus, diagnosing these types of faults is almost trivial. However, soft faults are not easily detectable because they are not only often confused with the usual fluctuations in system operation, but also have a slow, gradual impact on the productivity of the photovoltaic installation. Fault diagnosis and condition monitoring are important to increase the efficiency and reliability of photovoltaic modules [7]. The fault detection methods are divided into two types: model-based or model-free [6]. Model-based fault detection originated with Beard in 1971 in order to replace hardware redundancy with analytical redundancy [8]. It includes signal techniques, state estimators, parity space methods, and parameter estimation [9]. Based on the model, fault detection techniques are proposed to observe residual elements among the measured outputs of the practical systems and the model-estimated outputs [10], [11].

Fault Detection and Isolation (FDI) has been widely reported in various applications of power electronic systems, such as electric conversion systems, electric vehicles [1], [12], [13], [14]. Several nonlinear control approaches have been proposed for grid-tied power converters, such as nonlinear adaptive control, passivity-based control, model predictive control, and sliding mode control [15], [16], [17], [18], [19]. There are various works reported in the literature about the PV fault diagnosis [20], [21].

The observer-based fault diagnosis has been widely reported in various applications of power electronic systems, such as motor drives, electric conversion systems, electric vehicles [1], [22], [23], [24], [25]. The choice of diagnosis by the observer method based on active rejection of disturbances is justified by the fact that, on the one hand, the active disturbance rejection control considers non-linearities and uncertainties as disturbances, estimates and compensates for them. On the other hand, the extended-state-observer (ESO) method was designed for the ADRC to produce a compensation term in a simple and efficient way [4]. Once, in contrast to many control strategies, linear active disturbance rejection control (LADRC) is an independent method that does not depend on the exact mathematical model of the controlled system, which qualifies it for wide use in many practical applications and theoretical studies [3].

Photovoltaic systems, like other industrial systems, are subject to faults during operation. Several methods for detecting faults in photovoltaic (PV) systems exist in the literature. However, the criteria that these methods address, such as accuracy, speed, reliability, and robustness, are still under investigation. In addition, the applicability of the algorithms and methods developed varies according to the operating conditions of the

systems. Each diagnostic method has its own advantages and disadvantages. Because many uncertainties in photovoltaic systems are unmeasurable, the estimation-based diagnosis technique is particularly crucial. This paper aims to contribute to photovoltaic systems' fault diagnosis based on state estimation and residual analysis**.** This work contributes to PV diagnosis using state estimation and residual analysis approaches. Unlike other analytical approaches limited by their complexity and sensitivity to uncertainties, and considering non-linear systems such as PV systems, the proposed method not only takes into account the simultaneous detection of DC and AC fault sides, but also incorporates active disturbance rejection control, which ensures the stability of the technique.

The following sections explain this paper. The methods in Section 2 consist of the mathematical model, the proposed fault diagnosis approach, the state estimation, and residuals analysis approaches used in this study. Section 3 presents the simulation results before concluding the paper in Section 4.

2. Methods

2.1. Mathematical Model

The literature deals with several typologies of photovoltaic systems. This work is concerned with a photovoltaic system connected to a single-phase grid, considered as the load. The description provided by the equivalent electrical model in Figure 1 highlights the features and illustrates the different phases of system operation.

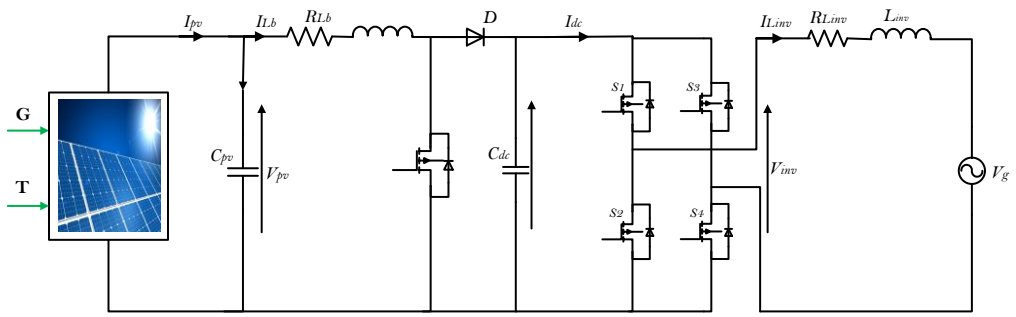

Figure 1. The system's electrical equivalent model.

The equivalent circuit above consists of a DC side and an AC side. The DC side is composed of a PV generator, a boost converter, and the DC bus. The AC side consists of a single-phase inverter, a filter *L,* and the grid part represented by the voltage V_g. Energy is released from the DC section to the AC section via the DC bus by the power switch S_b (MOSFET, IGBT) coupled to the diode *D*. The PWM modulator controls both the DC and AC converters by generating pulses with a frequency of $f=1/T$ and a width of μT, where $\mu \in [0, 1]$ represents the duty cycle of the control pulses.

Two phases illustrate the equivalent electrical model, and each one is described by two different conduction sequences.

1. The energy accumulation phase: during this phase, energy is accumulated in the smoothing inductor L_b, and it is described by the two conduction sequences below:
    i. Conduction sequence 1**:** during this sequence, the power switch S_b is ON while diode *D* is OFF (we consider the converter duty cycle $\mu_1=1$); and the inverter switches S_1, S_4 are ON while S_2, S_3 are OFF (we consider the inverter duty cycle, $\mu_2=1$).

ii. Conduction sequence 2: during this sequence, S_b is ON while D is OFF ($\mu_1=1$); and S_1, S_4 are OFF while S_2, S_3 are ON ($\mu_2=0$).

2. The energy transfer phase: During this phase, the energy stored in the inductance L_b is released into the load through the DC bus by the two conduction sequences below:

i. Conduction sequence 3: during this sequence, S_b is OFF and D is ON ($\mu_1=0$); and S_1, S_4 are ON and S_2, S_3 are OFF ($\mu_2=1$).

ii. Conduction sequence 4: during this sequence Sb is OFF and D is ON ($\mu_1=0$); and S_1, S_4 are OFF while S_2, S_3 are ON ($\mu_2=0$).

The average dynamic model deduced from the four conduction sequences is written as follows:

$$\begin{cases} \dfrac{dI_{Lb}}{dt} = -\dfrac{R_{Lb}}{L_b} I_{Lb} - \dfrac{(1-\mu_1)}{L_b} V_{dc\_bus} + \dfrac{V_{pv}}{L_b} \\ \dfrac{dV_{dc\_bus}}{dt} = \dfrac{(1-\mu_1)}{C_{dc}} I_{Lb} - \dfrac{(2\mu_2-1)}{C_{dc}} I_{inv} \\ \dfrac{dI_{inv}}{dt} = \dfrac{(2\mu_2-1)}{L_{inv}} V_{dc\_bus} - \dfrac{R_{Linv}}{L_{inv}} I_{inv} - \dfrac{V_g}{L_{inv}} \end{cases} \quad (1)$$

where Vpv is the voltage delivered by the PV module; ILb, RLb and Lb, are the current, the internal resistance, and the boost converter inductance respectively. Vdc_bus is the DC bus voltage. $Iinv$, $Rinv$, and $Linv$ are the current, resistance, and inductance inverters respectively. Vg is the grid voltage.

Let's put $x_1 = I_{Lb}$; $x_2 = V_{dc\_bus}$; $x_3 = I_{inv}$, Equation (1) becomes:

$$\begin{cases} \dot{x}_1(t) = -\dfrac{R_{Lb}}{L_b} x_1(t) - \dfrac{1}{L_b} x_2(t) + \dfrac{x_2(t)}{L_b}\mu_1 + \dfrac{V_{pv}}{L_b} \\ \dot{x}_2(t) = \dfrac{1}{C_{dc}} x_1(t) + \dfrac{1}{C_{dc}} x_3(t) - \dfrac{x_1(t)}{C_{dc}}\mu_1 - \dfrac{2x_3(t)}{C_{dc}}\mu_2 \\ \dot{x}_3(t) = -\dfrac{1}{L_{inv}} x_2(t) - \dfrac{R_{Linv}}{L_{inv}} x_3(t) + \dfrac{2x_2(t)}{L_{inv}}\mu_2 - \dfrac{V_g}{L_{inv}} \end{cases} \quad (2)$$

By setting the state, reference, and output variables $I_{Lb\_ref} = x_{1\_ref}(t)$; $V_{dc\_bus\_ref} = x_{2\_ref}(t)$; $I_{inv\_ref} = x_{3\_ref}(t)$; $x(t) = [I_{Lb}(t)\ V_{dc\_bus}(t)\ I_{inv}(t)]^T$; and $y(t) = [I_{Lb}\ V_{dc\_bus}\ I_{inv}]^T$, Equation (2) can be rewritten as:

$$\begin{cases} \dot{x}_1 = -\dfrac{R_{Lb}}{L_b} x_1(t) - \dfrac{1}{L_b} x_2(t) + \dfrac{x_{2\_ref}(t)}{L_b}\mu_1 + \left[\dfrac{V_{pv}}{L_b} + \left(\dfrac{x_2(t)}{L_b} - \dfrac{x_{2\_ref}(t)}{L_b}\right)\mu_1\right] \\ \dot{x}_2 = \dfrac{1}{C_{dc}} x_1(t) + \dfrac{1}{C_{dc}} x_3(t) - \dfrac{x_{1\_ref}(t)}{C_{dc}}\mu_1 - \dfrac{2x_{3\_ref}(t)}{C_{dc}}\mu_2 + \left[\left(-\dfrac{x_1(t)}{C_{dc}} + \dfrac{x_{1\_ref}(t)}{C_{dc}}\right)\mu_1 + \left(-\dfrac{2x_3}{C_{dc}} + \dfrac{2x_{3\_ref}(t)}{C_{dc}}\right)\mu_2\right] \\ \dot{x}_3 = -\dfrac{1}{L_{inv}} x_2(t) - \dfrac{R_{Linv}}{L_{inv}} x_3(t) + \dfrac{2x_{2\_ref}(t)}{L_{inv}}\mu_2 + \left[-\dfrac{V_g}{L_{inv}} + \left(\dfrac{2x_2(t)}{L_{inv}} - \dfrac{2x_{2\_ref}(t)}{L_{inv}}\right)\mu_2\right] \end{cases} \quad (3)$$

From Equation (3), the system operating in healthy mode can be modeled as follows:

$$\begin{cases} \dot{x}(t) = Ax(t) + B_1 u_1(t) + B_2 u_2(t) + E_d d(t,x,u) \\ y(t) = Cx(t) + Du(t) \end{cases} \quad (4)$$

where $A = \begin{pmatrix} -\frac{R_{Lb}}{L_b} & -\frac{1}{L_b} & 0 \\ \frac{1}{C_{dc}} & 0 & \frac{1}{C_{dc}} \\ 0 & -\frac{1}{L_{inv}} & -\frac{R_{inv}}{L_{inv}} \end{pmatrix}$ is the state matrix of the nominal system; $B_1 = \begin{pmatrix} \frac{1}{L_b} & 0 & 0 \\ 0 & -\frac{1}{C_{dc}} & 0 \\ 0 & 0 & 0 \end{pmatrix}$ and $B_2 = \begin{pmatrix} 0 & 0 & 0 \\ 0 & -\frac{2}{C_{dc}} & 0 \\ 0 & 0 & \frac{2}{L_{inv}} \end{pmatrix}$ are the control matrix of the nominal system; $C = I_{3\times3}$; $E_d = I_{3\times3}$; $D = 0_{3\times3}$

$$d(x,u,t) = \begin{pmatrix} d_1(x,u,t) \\ d_2(x,u,t) \\ d_3(x,u,t) \end{pmatrix} = \begin{pmatrix} \frac{V_{pv}}{L_b} + \left(\frac{x_2(t)}{L_b} - \frac{x_{2\_ref}(t)}{L_b}\right)\mu_1 \\ \left(-\frac{x_1(t)}{C_{dc}} + \frac{x_{1\_ref}(t)}{C_{dc}}\right)\mu_1 + \left(-\frac{2x_3}{C_{dc}} + \frac{2x_{3\_ref}(t)}{C_{dc}}\right)\mu_2 \\ -\frac{V_g}{L_{inv}} + \left(\frac{2x_2(t)}{L_{inv}} - \frac{2x_{2\_ref}(t)}{L_{inv}}\right)\mu_2 \end{pmatrix} \quad (5)$$

d(x,u,t) is a nonlinear function representing the nonlinearity of the system.

Remark 1. *The modelling of our system is divided into two parts. The first is a linear nominal part, characterised by the three nominal states I_{Lb}, V_{dc_bus} and I_{inv}. The second is a non-linear part, characterised by the three extended states d_1, d_2 and d_3, which are considered disturbances.*

Remark 2. *the ADRC command used in this work is intended to eliminate or mitigate the effects of disturbances.*

2.2. Proposed Fault Diagnosis Approach

For the purposes of this work, we assume that the internal parameters L_b, R_{Lb}, C_{dc}, L_{inv}, R_{Linv} do not vary. We are considering the following faults: disturbances at the input of the Boost converter coming from the photovoltaic panel are PV voltage variation and modelled as follows:

$$\bar{V}_{pv} = V_{pv0} + \Delta V_{pv} \quad (6)$$

We consider that the fault coming from the grid is the voltage variation. The grid voltage fault is modelled as follows:

$$\bar{V}_g = V_{g0} + \Delta V_g \quad (7)$$

PV voltage and grid voltage variation modify the extended states (disturbances). The disturbances d_1 are modified by the variation of the voltage V_{pv} of the PV generator as follows:

$$\bar{d}_1(x,u,t) = \frac{V_{pv0} + \Delta V_{pv}}{L_b} + \left(\frac{x_2(t)}{L_b} - \frac{x_{2\_ref}(t)}{L_b}\right)\mu_1 = \frac{\Delta V_{pv}}{L_b} + \left(\frac{V_{pv0}}{L_b} + \left(\frac{x_2(t)}{L_b} - \frac{x_{2\_ref}(t)}{L_b}\right)\mu_1\right) \quad (8)$$

Equation (8) takes the form:

$$\bar{d}_1(x,u,t) = d_1(x,u,t) + \Delta d_1(x,u,t) \quad (9)$$

with $d_1(x,u,t) = \left(\frac{V_{pv0}}{L_b} + \left(\frac{x_2(t)}{L_b} - \frac{x_{2\_ref}(t)}{L_b}\right)\mu_1\right)$, d_1 represents disturbances when the system is operating faultlessly; and $\Delta d_1(x,u,t) = \frac{\Delta V_{pv}}{L_b}$, Δd_1 denotes the disturbances variation.

The d_3 disturbances are modified by the variation of the network voltage V_g as follows:

$$\bar{d}_3(x,u,t) = \frac{V_{g0} + \Delta V_g}{L_{inv}} + \left(\frac{2x_2(t)}{L_{inv}} - \frac{2x_{2\_ref}(t)}{L_{inv}}\right)\mu_2 = \frac{\Delta V_g}{L_{inv}} + \left(\frac{V_{g0}}{L_{inv}} + \left(\frac{2x_2(t)}{L_{inv}} - \frac{2x_{2\_ref}(t)}{L_{inv}}\right)\mu_2\right) \quad (10)$$

$$\bar{d}_3(x,u,t) = d_3(x,u,t) + \Delta d_3(x,u,t) \quad (11)$$

with $\bar{d}_3(x,u,t) = \frac{V_{g0}}{L_{inv}} + \left(\frac{2x_2(t)}{L_{inv}} - \frac{2x_{2\_ref}(t)}{L_{inv}}\right)\mu_2$, d_3 represents disturbances when the system is operating faultlessly; and $\Delta d_3(x,u,t) = \frac{\Delta V_g}{L_{inv}}$, Δd_3 denotes the disturbances variation.

Equation (5)-(11) allow us to write the general form of the model of the failed system as follows:

$$\begin{cases} \dot{x}(t) = \bar{A}x(t) + \bar{B}\bar{u}(t) + E_d\bar{d}(t) \\ y(t) = \bar{C}x(t) + \bar{D}\bar{u}(t) + F_d\bar{d}(t) \end{cases} \quad (12)$$

To simplify the modelling of the faulty system, we have made a number of assumptions, as follows:

- We assume that the measuring sensors and the switch (*ST*) are faultless.
- The disturbances/defects considered are those that modify the passive chopper components, and those which modify the PV voltage and the grid voltage.

The disturbed model of the nominal system can be described by equation (13) as follows:

$$\begin{cases} \dot{x}(t) = Ax(t) + B_1u_1(t) + B_2u_2(t) + E_d\bar{d}(t) \\ y(t) = Cx(t) \end{cases} \quad (13)$$

with $\bar{d}(t) = d(t) + \Delta d(t), E_d = I_{3\times3}$; and $\bar{d}(x,u,t) = \begin{pmatrix} \bar{d}_1(x,u,t) \\ \bar{d}_2(x,u,t) \\ \bar{d}_3(x,u,t) \end{pmatrix} =$

$$\begin{pmatrix} \frac{\Delta V_{pv}}{L_b} + \left(\frac{V_{pv0}}{L_b} + \left(\frac{x_2(t)}{L_b} - \frac{x_{2\_ref}(t)}{L_b}\right)\mu_1\right) \\ \left(-\frac{x_1(t)}{C_{dc}} + \frac{x_{1\_ref}(t)}{C_{dc}}\right)\mu_1 + \left(-\frac{2x_3}{C_{dc}} + \frac{2x_{3\_ref}(t)}{C_{dc}}\right)\mu_2 \\ \frac{\Delta V_g}{L_{inv}} + \left(\frac{V_{g0}}{L_{inv}} + \left(\frac{2x_2(t)}{L_{inv}} - \frac{2x_{2\_ref}(t)}{L_{inv}}\right)\mu_2\right) \end{pmatrix}.$$

From the disturbed model, we can define the extended fault state model. The extended variables of the system are defined as follows:

$$\begin{cases} x_{n+1} = \bar{d}_1(t) \\ x_{n+2} = \bar{d}_2(t) \\ x_{n+3} = \bar{d}_3(t) \end{cases} \quad (14)$$

$$\begin{cases} h_1 = \dot{\bar{d}}_1(t) \\ h_2 = \dot{\bar{d}}_2(t) \\ h_3 = \dot{\bar{d}}_3(t) \end{cases} \quad (15)$$

The extended equation of state is written as:

$$\begin{cases} \dot{x}_e(t) = A_ex_e(t) + B_{e1}u_1(t) + B_{e2}u_2(t) + Eh(t) \\ y_e(t) = C_ex_e(t) \end{cases} \quad (16)$$

with $x_e(t) = \left[I_{Lb}(t)\ V_{dc\_bus}(t)\ I_{inv}(t)\ \bar{d}_1(t)\ \bar{d}_2(t)\ \bar{d}_3(t)\right]^T$; $u_1 = \begin{pmatrix} x_{2\_ref}(t)\cdot\mu_1 \\ x_{1\_ref}(t)\cdot\mu_1 \\ 0 \end{pmatrix}$; $u_2 = \begin{pmatrix} 0 \\ x_{3\_ref}(t)\cdot\mu_2 \\ x_{2\_ref}(t)\cdot\mu_2 \end{pmatrix}$; $h(t) = [h_1(t)\ h_2(t)\ h_3(t)]^T$. Ae, Be, and Ce are the state matrix, the control matrix, and the output matrix respectively on the extended system.

$$A_e = \begin{pmatrix} -\frac{R_{LBo}}{L_{bo}} & -\frac{1}{L_{bo}} & 0 & 1 & 0 & 0 \\ \frac{1}{C_{dco}} & 0 & 0 & 0 & 1 & 0 \\ 0 & -\frac{1}{L_{invo}} & -\frac{R_{Linvo}}{L_{invo}} & 0 & 0 & 1 \\ 0 & 0 & 0 & 0 & 0 & 0 \\ 0 & 0 & 0 & 0 & 0 & 0 \\ 0 & 0 & 0 & 0 & 0 & 0 \end{pmatrix}; \quad B_{e1} = \begin{pmatrix} \frac{1}{L_{bo}} & 0 & 0 \\ 0 & -\frac{1}{C_{dco}} & 0 \\ 0 & 0 & 0 \\ 0 & 0 & 0 \\ 0 & 0 & 0 \\ 0 & 0 & 0 \end{pmatrix};$$

$$B_{e2} = \begin{pmatrix} 0 & 0 & 0 \\ 0 & -\frac{2}{C_{dco}} & 0 \\ 0 & 0 & \frac{2}{L_{invo}} \\ 0 & 0 & 0 \\ 0 & 0 & 0 \\ 0 & 0 & 0 \end{pmatrix}; \quad C_e = [C \quad 0_{3\times3}]^T = \begin{pmatrix} 1 & 0 & 0 \\ 0 & 1 & 0 \\ 0 & 0 & 1 \\ 0 & 0 & 0 \\ 0 & 0 & 0 \\ 0 & 0 & 0 \end{pmatrix}; \quad E = \begin{pmatrix} 0 & 0 & 0 \\ 0 & 0 & 0 \\ 0 & 0 & 0 \\ 1 & 0 & 0 \\ 0 & 1 & 0 \\ 0 & 0 & 1 \end{pmatrix}.$$

The proposed GESO aims to estimate both the state variables I_{Lb}, V_{dc_bus}, I_{Linv} and the disturbances d_i, with I = 1, 2, 3;

$$\begin{cases} \dot{\hat{x}}_e(t) = A_e\hat{x}_e(t) + B_{e1}u_1(t) + B_{e2}u_2(t) + L(y - \hat{y}_e) \\ \hat{y}_e(t) = C_e\hat{x}_e(t) \end{cases} \tag{17}$$

with $\dot{\hat{x}}_e(t) = \left[\left(\hat{x}(t)\right)^T \quad \left(\hat{\bar{d}}(t)\right)^T\right]^T = \left[\hat{I}_{Lb}(t)\ \hat{V}_{dc\_bus}(t)\ \hat{I}_{inv}(t)\ \hat{\bar{d}}_1(t)\ \hat{\bar{d}}_2(t)\ \hat{\bar{d}}_3(t)\right]^T$, the estimated extended state.

2.3. State Estimation and Residual Analysis in PV Diagnostic Case Study

The logic of the diagnosis based on state estimation is as follows: once the nominal and extended states have been estimated, we can directly determine whether a fault has occurred or not by checking whether the estimated curve deviates from the actual curve. The fault detecting based on residuals analysis consist of generating the residuals between the actual and estimated values of the states when the system is operating in healthy and faulty conditions. Faults are detected if the residuals exceed the defined limit values. This section describe diagnosis by residual analysis.

The choice of threshold values is very decisive for fault detection. In general, the smaller the threshold, the shorter the detection time. However, a very low threshold value easily causes false alarms [26]. In the context of our work, let us define the threshold or limit values that allow fault detection as follows:

$$T = \sup\|R_o(t)\| \tag{18}$$

with $R_o(t)$ represents the residual vector when the system is operating faultlessly. Assuming a tolerance of 5% of the threshold value T, the accepted threshold value is shown in Equation (19).

$$T = 1.05 * \sup\|R_o(t)\| \tag{19}$$

Then, residuals r_1 is usually defined as the function of output estimation error [27], as seen in Equation (19).

$$R(t) = \|\varepsilon(t)\| \tag{20}$$

with $\varepsilon(t)$ defined as $x_e - \hat{x}_e = \begin{bmatrix} i_{Lb}(t) - \hat{\imath}_{Lb}(t) \\ v_{dc\_bus}(t) - \hat{v}_{dc\_bus}(t) \\ i_{inv}(t) - \hat{\imath}_{inv}(t) \\ d_1(t) - \hat{d}_1(t) \\ d_2(t) - \hat{d}_2(t) \\ d_3(t) - \hat{d}_3(t) \end{bmatrix}$. The threshold values are selected in two stages:

1. Stage 1: Generate the residuals between the actual and estimated values of the states when the system is in healthy operation. The upper limit values of these nominal threshold values are the system limit values.
2. Stage 2: Generate the residuals between the actual and estimated values of the states when the system is faulty. When these residuals exceed the limit values defined in step 1, faults are detected.

As mentioned in Remark 1, extended states reveal the system's nonlinearity and faults. These algorithms enable the detection and identification of faults.

1) Disturbance $\bar{d}_1$ residual analysis

The first component of the residual $\|R_{d1}(t)\|$ is related to the parameters V_{pv}, L_b, and R_b, assuming that the voltage V_{pv} is measurable, the parameters L_b (nominal inductance) and R_b (nominal resistance) are known. The detection and identification of faults by analyzing the $\bar{d}_1$ residuals are described by the following algorithm:

- Measure V_{pv}.
- Measure $\bar{d}_1$ or determine $\hat{\bar{d}}_1$.
- Calculate the voltage variation V_{pv}: $\Delta V_{pv} = |V_{pv} - V_{pv0}|$.
- Calculate the residual $\|R_{d1}\| = \left|d_1 - \hat{\bar{d}}_1\right|$.
  - If $\|R_{d1}\| < \alpha_1$ (with α_1 the threshold value of the disturbance d_1 residual, obtained in nominal operation), then the system is not faulty.
  - If $\|R_{d1}\| > \alpha_1$, the system is faulty.
    - If $\Delta V_{pv} = 0$, then the system is faulty due to its parameters L_b and/or R_b; this is referred to converter fault.
    - If $\Delta V_{pv} \neq 0$, then check the quantity $\|R_{d1}\| - \Delta V_{pv}/L_b$.
      - If $\|R_{d1}\| - \Delta V_{pv}/L_b \approx 0$, the fault comes from the PV generator.
      - If $\|R_{d1}\| - \Delta V_{pv}/L_b \neq 0$, the fault comes from the PV generator and the failure of the boost converter parameters.

The disturbances $\bar{d}_1$ residual analysis allows identifying faults from the PV generator via the V_{pv} voltage, and faults from the boost converter via the L_b inductance.

2) Disturbance $\bar{d}_2$ residual analysis

The second component of the residual $\|R_{d2}(t)\|$ is related to the DC bus parameter C_{dc}, assuming that the nominal capacity C_{dc0} is known. The faults

detection and identification of faults by $\bar{d}_2$ residuals analysis is described as the following algorithm:

- Measure $\bar{d}_2$ or determine $\hat{\bar{d}}_2$.
- Calculate the residual $\|R_{d2}\| = \left|d_2 - \hat{\bar{d}}_2\right|$.
  - If $\|R_{d2}\| < \alpha_2$ (with α_2 the threshold value of the disturbance d_2 residual, obtained in nominal operation), then the system is not faulty.
  - If $\|R_{d2}\| > \alpha_2$, the system is faulty.
    - If $\Delta C_{dc} \neq 0$, then the system is faulty due to its parameters C_{dc}; this is referred to a DC bus fault.
    - If $\Delta C_{dc} = 0$, then the fault is from the PV generator and from the other system parameters failure.

The disturbances $\bar{d}_2$ residual analysis can be used to identify DC bus faults through the capacitance.

3) Disturbance $\bar{d}_3$ residual analysis

The third component of the residual $\|R_{d3}(t)\|$ is related to the parameters V_g, L_{inv}, and R_{Linv}, assuming that the voltage V_g is measurable, the parameters L_{inv} (nominal inductance) and R_{Linv} (nominal resistance) are known. The detection and identification of faults by analyzing the $\bar{d}_3$ residuals are described by the following algorithm:

- Measure V_g.
- Measure $\bar{d}_3$ or determine $\hat{\bar{d}}_3$.
- Calculate the voltage variation V_g: $\Delta V_g = \left|V_g - V_{g0}\right|$.
- Calculate the residual $\|R_{d3}\| = \left|d_3 - \hat{\bar{d}}_3\right|$.
  - If $\|R_{d3}\| < \alpha_3$ (with α_3 the threshold value of the disturbance d_3 residual, obtained in nominal operation), then the system is not faulty.
  - If $\|R_{d3}\| > \alpha_3$, the system is faulty.
    - If $\Delta V_g = 0$, then the system is faulty due to its parameters L_{inv} and/or R_{Linv}; this is referred to filter fault.
    - If $\Delta V_g \neq 0$, then check the quantity $\|R_{d3}\| - \Delta V_g / L_{inv}$.
      - If $\|R_{d3}\| - \Delta V_g / L_{inv} \approx 0$ and $\Delta L_{inv} \approx 0$, the fault comes from the network.
      - If $\|R_{d3}\| - \Delta V_g / L_{inv} \neq 0$ and $\Delta L_{inv} \neq 0$, the fault comes from the network and the filter failure.

The disturbances $\bar{d}_3$ residual analysis allows identifying faults from grid via the V_g voltage, and faults from the filter via the L_{inv} inductance.

3. Results and Discussion

3.1. Residual Generation and Threshold Selection

For the purposes of this study, an error of 5% is permitted and we will assume that the fault detection system is sensitive to estimation errors exceeding 5%. The 5% threshold was selected according to experimental performed in the literature where a statistical analysis of noise under nominal operating conditions shows that 95% of errors remain below 5%. This choice was also motivated by the need to strike an optimal balance between the detection rate, non-detection rate, and false alarm rate. Furthermore, when considering the inherent uncertainties associated with variations in irradiance, as well as

the imperfections of the model and the sensors, a threshold of 5% between normal and abnormal operation is considered realistic in a PV system.

Assuming a tolerance of 5%, the residuals of the states and disturbances obtained during normal operation are used to define the residual thresholds according to the following table.

Table 1. Residual and threshold values, tolerance 5%.

Residual	Threshold Value
R_1 (R_{ILb}) = 49.56 × 10^{-4}	T_1 (R_{ILb}) = 52.03 × 10^{-4}
R_2 (R_{Cdc_bus}) = 41 × 10^{-2}	T_2 (R_{Cdc_bus}) = 43.05 × 10^{-2}
R_3 (R_{Iinv}) = 6.6 × 10^{-8}	T_3 (R_{Iinv}) = 6.93 × 10^{-8}
R_4 (R_{d1}) = 45.75	T_4 (α_1) = 48.03
R_5 (R_{d2}) = 375.8	T_5 (α_2) = 394.59
R_6 (R_{d3}) = 5.1 × 10^{-5}	T_6 (α_3) = 5.36 × 10^{-5}

3.2. Faults Diagnosis Due to Photovoltaic Voltage Variation

Assume that the PV generator voltage *Vpv* changes according to the effects of shading demonstrated by [28], [29], as seen in Table 2.

Table 2. PV voltage changes due to shading effects.

Time (s)	Voltage (V)
0 ≤ t ≤ 0.2	120
0.2 < t ≤ 0.4	53.01
0.4 < t ≤ 0.6	50.87
0.6 < t ≤ 1	53.01
1 < t ≤ 1.2	120
1.2 < t ≤ 1.4	53.01
1.4 < t ≤ 1.6	52.60
1.6 < t ≤ 1.8	120
1.8 < t ≤ 2	50.14

Faults detection when the system is subjected to a voltage variation is shown in Figure 2 and 3. Despite variations in the V_{pv} voltage, Figure 2(a) shows how the estimated I_{Lb} current follows the actual current. However, it is evident that the I_{Lb} current varies with the V_{pv} voltage. Residual analysis of the actual and estimated currents reveals the presence of peaks of the order of 0.12A with variation times of 0.2s, 1 s, 1.2s, 1.6s and 1.8s greater than the T_1 threshold. As Figure 2(b) clearly shows, the presence of these peaks is indicative of faults at these times. The lack of fault detection at 0.4s, 0.6s and 1.4s would be due to the low external disturbances, which are of order of 2.14V and 0.41V. Looking closely at the actual and estimated current curves shown in figure 8a, it is difficult to see any shift in the varying times. Only residual synthesis can be used for fault detection in this case.

Figure 2(c) shows that the estimated V_{dc_bus} curve normally follows the real curve, even when V_{pv} varies. By simply observing the estimated curve, fault is undetectable. However, the residuals synthesis in Figure 2(d) shows fault with the presence of a peak of order 0.437V above the T_2 threshold at 1.82s. This confirms the assumption that the lower the threshold, the faster the detection. Figure 2(f) shows that at times 0.24s, 044s, 0.97s and 1.95s the I_{inv} current is affected by the variation of the V_{pv} voltage. Analyzing the residuals shows that the presence of peaks exceeding T_3 threshold at these times

indicates the fault. Since the estimated curve follows the actual curve correctly, fault is undetectable by observing the estimated I_{inv} curve.

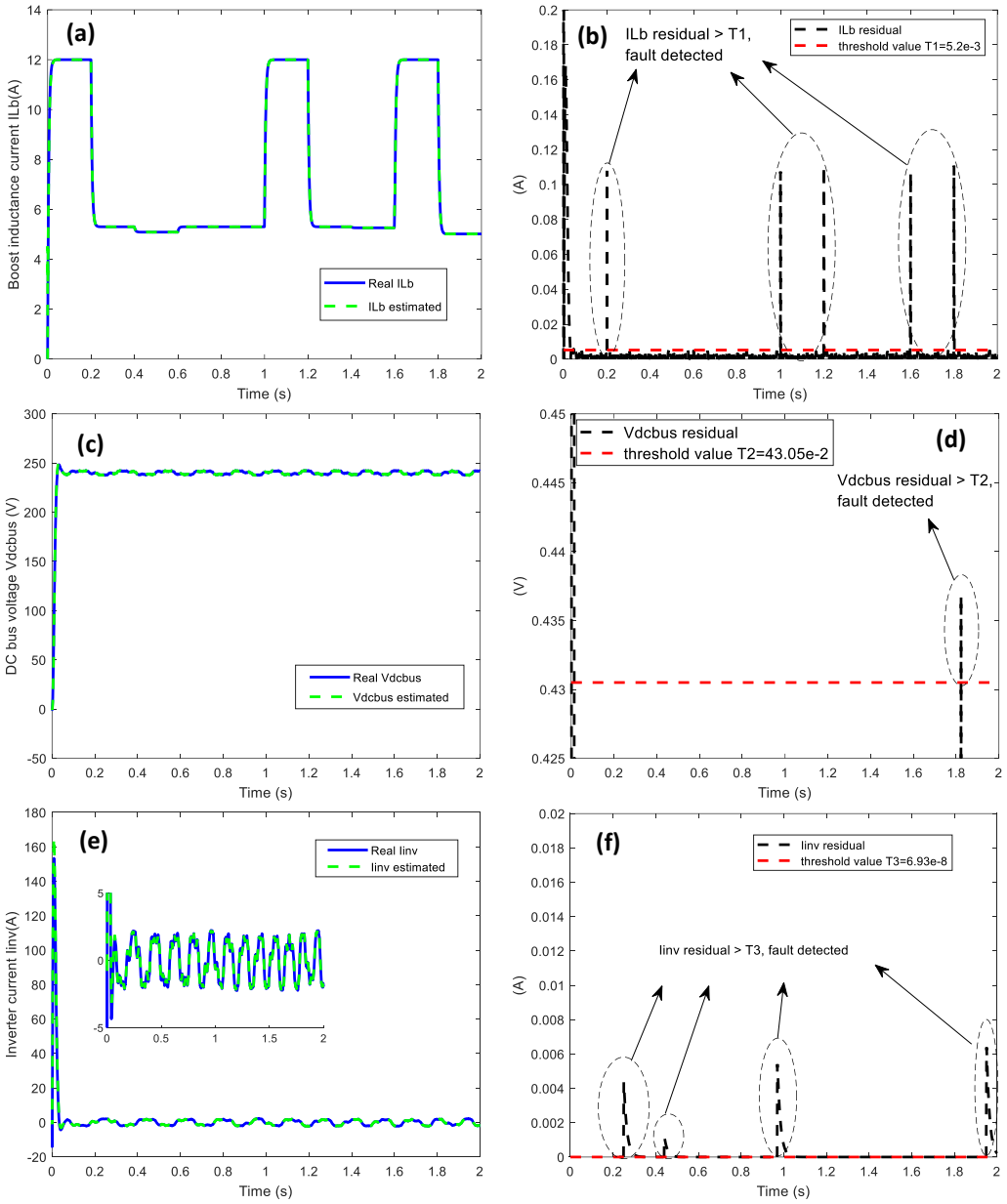

Figure 2. Faults detection when the system is subjected to a PV voltage variation V_{pv}: **(a)** estimating the current I_{Lb}, **(b)** analyzing the residual R_1, **(c)** estimating the V_{dc_bus} voltage, **(d)** analyzing the residual R_2, **(e)** estimating the current I_{inv}, and **(f)** analyzing the residual R_3.

The voltage variation V_{pv} affects the nominal disturbance d_1. Figure 3(a) gives a good estimate of d_1. But for the 0.2s and 1.8s times, there is some shift between the actual and estimated d_1 curves. In this case, the proposed method can detect faults in the system by estimating the disturbance. There are peaks of about 1400 at times 0.2s, 1s, 1.2s, 1.6s and 1.8s in the residual synthesis curve shown in Figure 3(b). These peaks above the T_4 threshold indicate the presence of faults at these times. The small perturbations at 0.4s, 0.6s and 1.4s of the order of 2.14V and 0.41V are not sufficient for fault detection. Reducing the threshold by a tolerance of less than 5% applied to the R_4 residual would detect small amplitude faults.

No faults are detected on the nominal disturbance d_2 estimation curve and the residual R_5 analysis shown in Figure 3(c) and (d). The analysis of these curves indicates that the system is functioning flawlessly. The 5% residual threshold seems very high for this scenario.

Figure 3(e) shows that at times 0.2s, 0.4s, 0.9s and 1.9s there is a shift between the actual and estimated curves of the nominal disturbance d_3. This shift indicates disturbances at these times. Thus, when there are faults in the system, it can be observed by estimating the nominal disturbance d_3. In Figure 3(f), we observe peaks of the order of 10.6, 2.34, 13 and 15 at the times 0.2 s, 0.4 s, 0.97 s and 1.95 s above the threshold T_6. The system is faulty at these times of V_{pv} voltage variation, as shown by the d_1 disturbances residual synthesis.

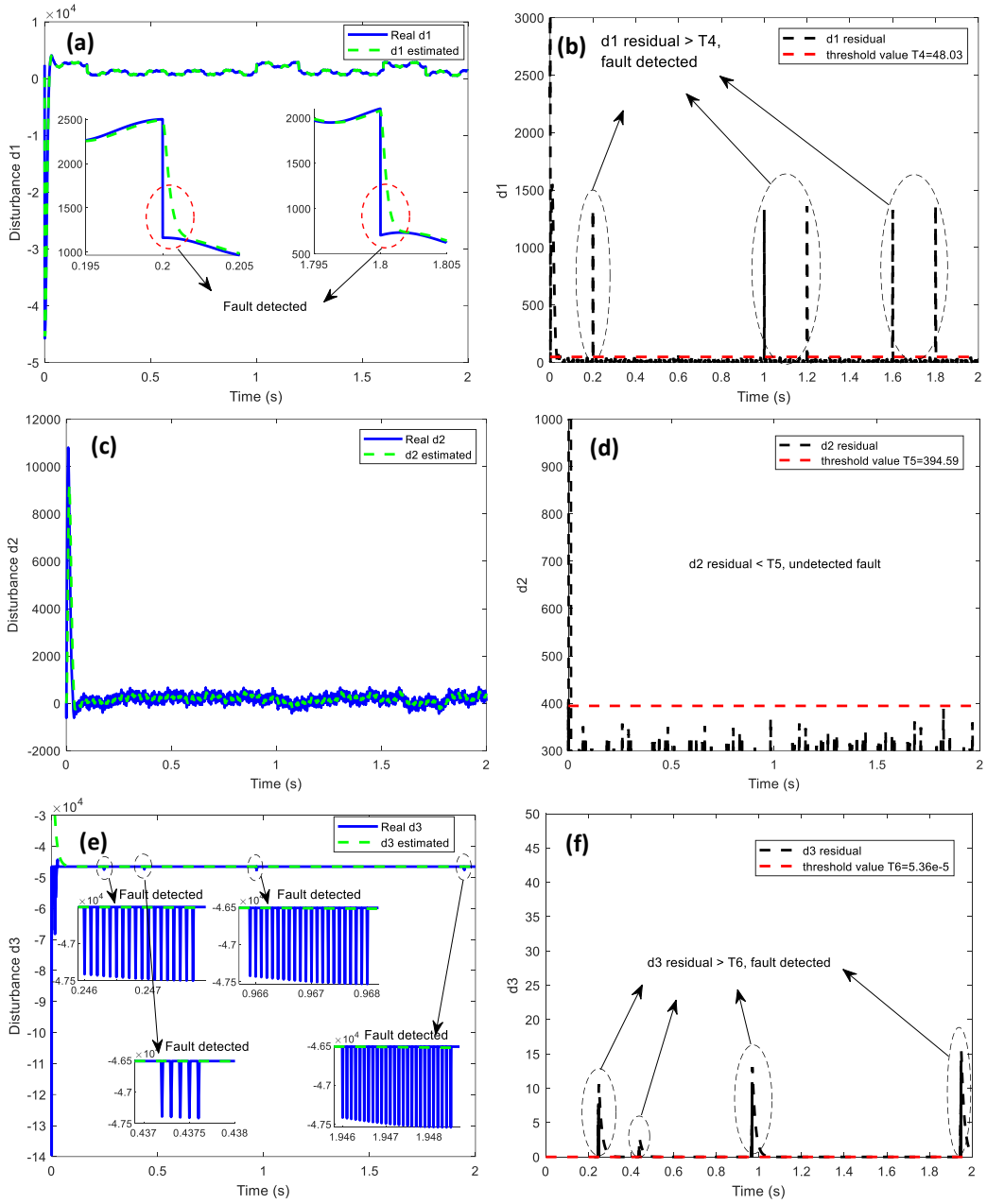

Figure 3. Faults detection when the system is subjected to a PV voltage variation V_{pv}:
(a) estimating disturbance d_1, **(b)** analyzing the residual R_4, **(c)** estimating disturbance d_2, **(d)** analyzing the residual R_5, **(e)** estimating disturbance d_3, **(f)** analyzing the residual R_6.

3.3. Faults Diagnosis Due to Grid Voltage Variation

Assume that the V_g voltage changes as shown in Table 3.

Table 3. Grid voltage changes assumption in this study.

Time (s)	Voltage (V)
0 ≤ t ≤ 0.2	240
0.2 < t ≤ 0.4	180
0.4 < t ≤ 0.6	160
0.6 < t ≤ 1	220
1 < t ≤ 1.2	280
1.2 < t ≤ 1.4	380
1.4 < t ≤ 1.6	240
1.6 < t ≤ 1.8	110
1.8 < t ≤ 2	380

Figure 8 shows fault detection by estimating the I_{Lb} current and analyzing its residual during the V_g voltage changing. Figure 8a shows that the estimated curve differs from the real curve at times 0.2 s, 0.4 s, 0.6 s, 1 s, 1.2 s, 1.4 s, 1.6 s and 1.8 s during the V_g voltage. As the V_g voltage increases, the estimated curve shifts downwards. When the V_g voltage decreases, the estimated curve shifts upwards. From these observations we can conclude that the proposed method enables fault detection by state estimation. Analysis of the residuals in Figure 8b shows that faults are detected by the presence of peaks between 0.01A and 0.17A, above the threshold T_1.

Figure 9a shows a good V_{dc_bus} voltage estimation. The estimated curve follows the actual curve well. Slight shifts between the actual and estimated curves can be seen by zooming in at times 0.6s, 1.6s and 1.8s, indicating the presence of an error. The residual analysis in Figure 9b shows peaks in the order of 0.8V to 7.8V, well above the threshold T_2. This indicates the presence of a fault.

Estimating the state of I_{inv} in Figure 10a reveals the faults at the V_g voltage variation times (0.6s, 1.2s, 1.4s and 1.8s) by the shift between the real and estimated curves. The residual R_3 analysis indicates the presence of faults at the variation times by the peaks above the threshold T_3.

The estimations of the disturbances d_1, d_2 and d_3 and the residuals analysis are shown in figures 11 to 13. Through the estimation of the extended states d_2 and d_3, figures 12a and 13a show the faults detection at the V_g voltage variation times of by a shift between the real estimated and curves. Analyzing the residuals R_4, R_5 and R_6 allows faults to be detected by the presence of peaks at V_g variation times greater than the thresholds T_4, T_5 and T_6.

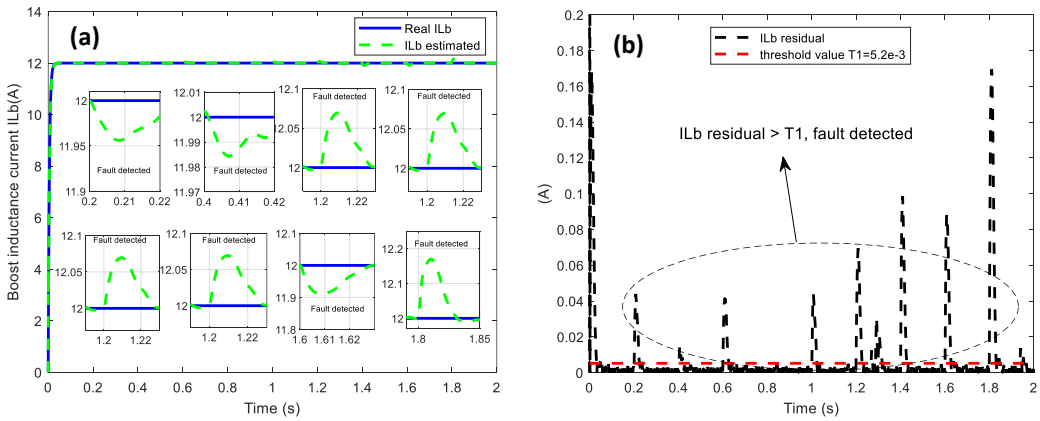

Figure 4. Faults detection when the system is subjected to a grid voltage variation V_g: **(a)** estimating the current I_{Lb}, **(b)** analyzing the residual R_1, **(c)** estimating V_{dc_bus} voltage, **(d)** analyzing the residual R_2, **(e)** estimating I_{inv} current, **(f)** analyzing the residual R_3, **(g)** estimating

disturbance d_1, **(h)** analyzing the residual R_4, **(i)** estimating disturbance d_2, **(j)** analyzing the residual R_5, **(k)** estimating disturbance d_3, **(l)** analyzing the residual R_6.

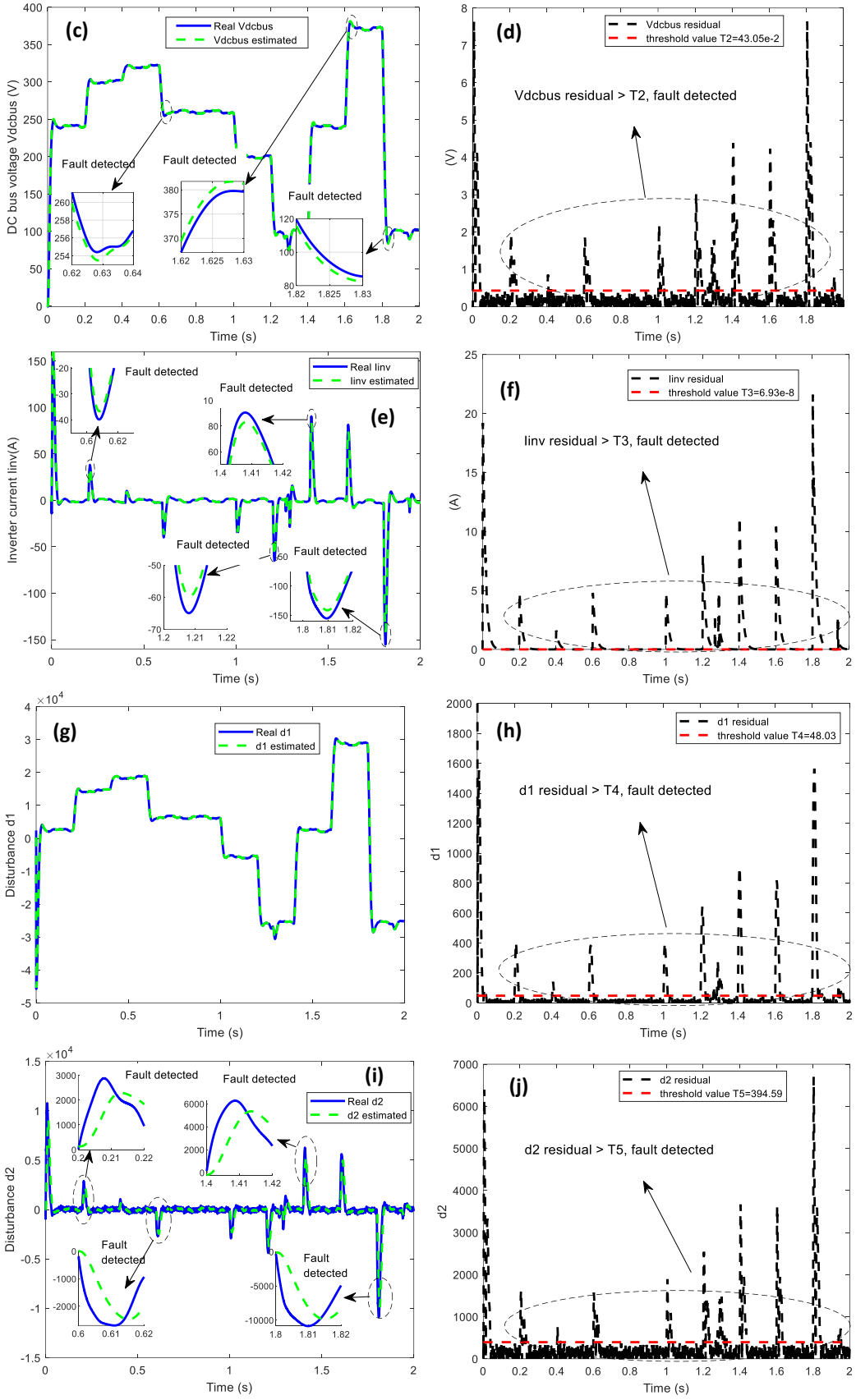

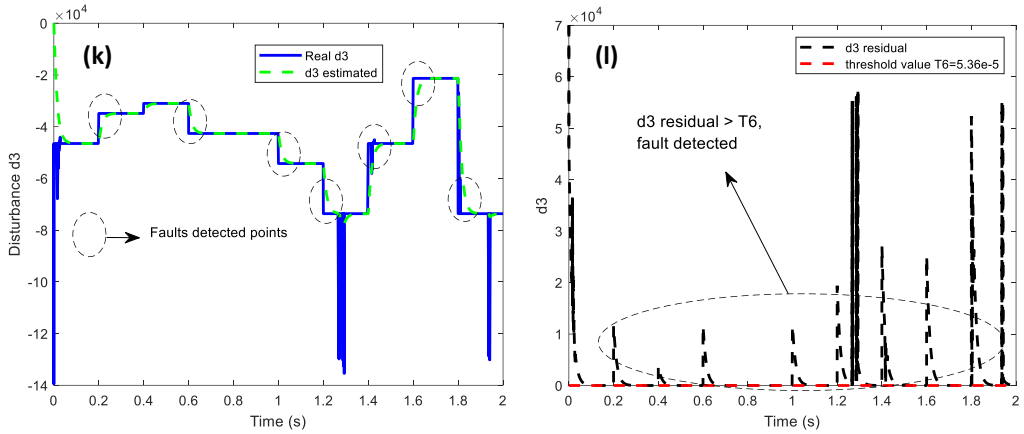

3.4. Diagnosis Performance Analysis

We subjected our system PV and grid voltages variation and defined eight occurrence fault points, assuming that if the system detects faults at all eight disturbance points, the detection tool is considered 100% sensitive. This study assumed that the number of undetected disturbance points determines the non-detection rate (NDR) is defined in equation 21.

$$NDR = \frac{UFN}{DFN + UFN} \times 100 \tag{21}$$

where UFN is the undetected faults number and DFN the detected faults number. Another assumption is that the false alarm rate is defined by peaks appearing above the 5% threshold at the undefined occurrence fault points. When the system is subjected to PV voltage variation, Table 4 describes the diagnostic performance.

Table 4. Diagnosis performance analysis under V_{pv} variation. With a fault detection rate of 62.5%, the I_{Lb} current and disturbance d_1 parameters have the highest sensitivity. Faults with very low amplitudes are not detected.

Estimated Parameter	Detection Rate (%)	False Alarm Rate (%)
I_{Lb}	62.5	0.00
V_{dc_bus}	12.5	0.00
I_{inv}	50.0	0.00
d_1	62.5	0.00
d_2	0.0	0.00
d_3	50.0	0.00

Table 4 shows that state I_{Lb} and disturbance d_1 have the same sensitivity and non-detection rate, as do state I_{inv} and disturbance d_3. This confirms the fact that disturbances d_1 and d_3 are strongly influenced by the parameters V_{pv} and V_g, respectively; which are the sources of the faults studied in this work (equation 5). The 0% detection rate in the d_2 disturbance analysis can be explained by the fact that, according to equation 5, this parameter is not significantly affected by variations in the V_{pv} and V_g voltages. However, the d_2 disturbance is closely linked to the power transfer switch S_b which, together with the transfer diode, ensures the transfer of energy to the load; to the AC-side PWM modulator, and to the DC bus capacitor. Hence, faults arising from these parameters could therefore be easily detected by analyzing the spectrum of the d_2 disturbance. The low sensitivity of the system in detecting PV source faults using V_{dc} state residual analysis could concern the effectiveness of the MPPT algorithm related.

Table 5. Diagnosis performance analysis under V_g variation. The estimation of all nominal and extended parameters is instrumental faults at all points of disturbance.

Estimated Parameter	Detection Rate (%)	False Alarm Rate (%)
I_{Lb}	100	25.0
V_{dc_bus}	100	25.0
I_{inv}	100	25.0
d_1	100	25.0
d_2	100	25.0
d_3	100	25.0

As shown in the table 5, with a threshold of 5%, the diagnostic tool can detect all faults caused by variations in V_g voltage when estimating all nominal and extended states. While the tool is sensitive, it should be noted that the false alarm rate of 25% must be eliminated. Based on the analysis of the diagnoses presented in tables 2 and 3, we can conclude that the diagnostic tool responds differently to faults originating from the PV and grid sides. However, to eliminate the observed false alarm rate in table 5, the defined residue threshold for detecting faults originating from the network must be reviewed by reassessing the fixed threshold and adjusting it using an adaptive threshold based on the system's operating conditions. Furthermore, we propose reducing erroneous fluctuations by incorporating a signal smoothing system, such as a Kalman filter. Another approach we propose involves integrating a dual-validation system, whereby an alarm can only be triggered if two independent conditions are met.

Assuming that sensors and switches are fault-free, and that a single 5% threshold is applied to the entire fault detection system, the results of this study show that faults are detected through an analysis of the estimation curves and an analysis of the residuals. However, the related works in [10], [22], and [26], switches and sensors are the subject of diagnosis. Within the framework of this work, six parameters (three nominal and three extended) are analyzed to determine their sensitivity to the presence of faults. This approach offers a wide range of options for selecting the most suitable parameter to verify the health of the system. As presented in the related works in [10], [22], and [26], the residual generation process is derived from the analysis of the system behavior in healthy and faulty modes of operation. The table 6 presents a brief comparison between this study and the works of the three authors cited above, emphasizing their main differences.

Real-world photovoltaic installations are subject to environmental factors, noise, measurement uncertainties, sensor imperfections and switching faults, which simulations often fail to reproduce. This is why experimental validation would help to bridge the gap between simulation assumptions and the system's actual operating conditions. However, experimental validation was not performed in this study. In theory, we wanted to validate our diagnostic model within a system that considers both DC and AC components, thereby addressing the limitations identified in the literature. Furthermore, the working conditions under which this study was conducted prevented us from setting up a test bench for developing an experimental prototype, and accessing field data was not straightforward. Since the objective of this study is to demonstrate the theoretical feasibility of the proposed model, subsequent research will be conducted to quantify the gap between simulation assumptions and real-world deployment conditions and the simulation results presented in this work point to future experimental work.

Table 6. Brief comparison contrasting the proposed approach with the three related works.

Ref.	Fault Detection Approach	Residual Generation	Numbers of Parameter	Type of Fault Considered	Application
[10]	Observers and residual generation	Under healthy and faulty modes	2 parameters (current sensor and dc link voltage sensor)	Catenary current sensor and dc link voltage sensor	Electrical railway traction
[22]	Nonlinear Luenberger observers and directional residual evaluation	Under healthy and faulty modes	3 parameters (nominal control voltages)	open-switch faults	Induction Motor Drives
[26]	Luenberger observer	Under healthy and faulty modes	1 parameter (inductor current)	Switch fault	DC-DC converter for cell application
Proposed method	State estimation-based observer (with Active Disturbance Rejection Control) and residual analysis	Under healthy and faulty modes	6 parameters (inductance current, dc link volage, inverter current, and 3 disturbances parameters	PV side faults and grid side fault	Single-Phase Grid connected PV system

4. Conclusions

This paper highlights a fault diagnosis for a Single-Phase Grid connected PV system subjected to photovoltaic generator and grid voltage variations. After developing the system's mathematical model, the Extended State Observer is used to estimate the system states and uncertainties due to modelling errors modelled as extended states. Two fault diagnosis approaches are used in this work: the state estimation and the residual analysis approaches. When the system is subjected to PV voltage variation, faults are detected by observing two extended states (d_1 and d_3) estimation curves. Faults resulting from variations in the grid voltage can be identified by examining the estimation curves for the three nominal states I_{Lb}, V_{dcbus} and I_{inv} and the two extended states d_2 and d_3. We applied a tolerance of 5% to the residuals of the nominal and extended states. Faults are detected by the presence of residual peaks above threshold. Analysis of the residual curves indicates that 65% of faults from the PV source are detected. The I_{Lb} current and disturbance d_1 parameters have the highest sensitivity. The non-detection rate varies according to the amplitude of the fault. Faults with very low amplitudes go undetected. Faults originating from the network are detected 100% of the time by analysing all nominal and extended states. However, 25% of false alarms are observed. These results suggest that analysing nominal and extended state estimation curves to diagnose faults is limited. This is because faults that are detectable by the deviation between the actual curve and the estimated curve are easily observable for large amplitude disturbances. Meanwhile, residual analysis provides an excellent fault diagnosis. However, it is important to be cautious when selecting the threshold value to avoid an excessive number of false alarms or missed detection.

Funding: This research received no external funding.

Data Availability Statement: The data that support the findings of this study are available from the corresponding author upon reasonable request.

Acknowledgments: The authors would like to acknowledge the support from Department of Renewable Energy, National Advance School of Engineering, of Maroua, University of Maroua.

Conflicts of Interest: The authors declare no conflicts of interest.

References

[1] Z. Yang and Y. Chai, "A survey of fault diagnosis for onshore grid-connected converter in wind energy conversion systems," *Renewable and Sustainable Energy Reviews*, vol. 66, pp. 345–359, Dec. 2016, doi: 10.1016/j.rser.2016.08.006.

[2] Q. Navid, A. Hassan, A. A. Fardoun, R. Ramzan, and A. Alraeesi, "Fault Diagnostic Methodologies for Utility-Scale Photovoltaic Power Plants: A State of the Art Review," *Sustainability*, vol. 13, no. 4, p. 1629, Feb. 2021, doi: 10.3390/su13041629.

[3] A. A. Smadi, F. Khoucha, Y. Amirat, A. Benrabah, and M. Benbouzid, "Active Disturbance Rejection Control of an Interleaved High Gain DC-DC Boost Converter for Fuel Cell Applications," *Energies (Basel).*, vol. 16, no. 3, p. 1019, Jan. 2023, doi: 10.3390/en16031019.

[4] J. She, K. Miyamoto, Q.-L. Han, M. Wu, H. Hashimoto, and Q.-G. Wang, "Generalized-Extended-State-Observer and Equivalent-Input-Disturbance Methods for Active Disturbance Rejection: Deep Observation and Comparison," *IEEE/CAA Journal of Automatica Sinica*, vol. 10, no. 4, pp. 957–968, Apr. 2023, doi: 10.1109/JAS.2022.105929.

[5] F. Bizzarri, A. Brambilla, L. Caretta, and C. Guardiani, "Monitoring performance and efficiency of photovoltaic parks," *Renew. Energy*, vol. 78, pp. 314–321, Jun. 2015, doi: 10.1016/j.renene.2015.01.002.

[6] J. Poon, P. Jain, I. C. Konstantakopoulos, C. Spanos, S. K. Panda, and S. R. Sanders, "Model-Based Fault Detection and Identification for Switching Power Converters," *IEEE Trans. Power Electron.*, vol. 32, no. 2, pp. 1419–1430, Feb. 2017, doi: 10.1109/TPEL.2016.2541342.

[7] A. Haque, K. V. S. Bharath, M. A. Khan, I. Khan, and Z. A. Jaffery, "Fault diagnosis of Photovoltaic Modules," *Energy Sci. Eng.*, vol. 7, no. 3, pp. 622–644, Jun. 2019, doi: 10.1002/ese3.255.

[8] Q. Su, C. Li, X. Guo, X. Zhang, and J. Li, "Robust fault diagnosis for DC–DC Boost converters via switched systems," *Control Eng. Pract.*, vol. 112, p. 104836, Jul. 2021, doi: 10.1016/j.conengprac.2021.104836.

[9] S. X. Ding, *Model-based Fault Diagnosis Techniques*. Berlin, Heidelberg: Springer Berlin Heidelberg, 2008. doi: 10.1007/978-3-540-76304-8.

[10] A. Ben Youssef, S. K. El Khil, and I. Slama-Belkhodja, "State Observer-Based Sensor Fault Detection and Isolation, and Fault Tolerant Control of a Single-Phase PWM Rectifier for Electric Railway Traction," *IEEE Trans. Power Electron.*, vol. 28, no. 12, pp. 5842–5853, Dec. 2013, doi: 10.1109/TPEL.2013.2257862.

[11] J. Li, K. Pan, D. Zhang, and Q. Su, "Robust fault detection and estimation observer design for switched systems," *Nonlinear Analysis: Hybrid Systems*, vol. 34, pp. 30–42, Nov. 2019, doi: 10.1016/j.nahs.2019.05.001.

[12] J. Blesa, D. Rotondo, V. Puig, and F. Nejjari, "FDI and FTC of wind turbines using the interval observer approach and virtual actuators/sensors," *Control Eng. Pract.*, vol. 24, pp. 138–155, Mar. 2014, doi: 10.1016/j.conengprac.2013.11.018.

[13] N. M. A. Freire, J. O. Estima, and A. J. M. Cardoso, "A New Approach for Current Sensor Fault Diagnosis in PMSG Drives for Wind Energy Conversion Systems," *IEEE Trans. Ind. Appl.*, vol. 50, no. 2, pp. 1206–1214, Mar. 2014, doi: 10.1109/TIA.2013.2271992.

[14] E. Ribeiro, A. J. M. Cardoso, and C. Boccaletti, "Open-Circuit Fault Diagnosis in Interleaved DC–DC Converters," *IEEE Trans. Power Electron.*, vol. 29, no. 6, pp. 3091–3102, Jun. 2014, doi: 10.1109/TPEL.2013.2272381.

[15] Y. Wang, Y. Lu, and R. Xiao, "Application of Nonlinear Adaptive Control in Temperature of Chinese Solar Greenhouses," *Electronics (Basel).*, vol. 10, no. 13, p. 1582, Jun. 2021, doi: 10.3390/electronics10131582.

[16] Z. Hekss, A. Abouloifa, I. Lachkar, F. Giri, S. Echalih, and J. M. Guerrero, "Nonlinear adaptive control design with average performance analysis for photovoltaic system based on half bridge shunt active power filter," *International Journal of Electrical Power & Energy Systems*, vol. 125, p. 106478, Feb. 2021, doi: 10.1016/j.ijepes.2020.106478.

[17] M. Hassan, C.-L. Su, F.-Z. Chen, and K.-Y. Lo, "Adaptive Passivity-Based Control of a DC–DC Boost Power Converter Supplying Constant Power and Constant Voltage Loads," *IEEE Transactions on Industrial Electronics*, vol. 69, no. 6, pp. 6204–6214, Jun. 2022, doi: 10.1109/TIE.2021.3086723.

[18] M. Schwenzer, M. Ay, T. Bergs, and D. Abel, "Review on model predictive control: an engineering perspective," *The International Journal of Advanced Manufacturing Technology*, vol. 117, no. 5–6, pp. 1327–1349, Nov. 2021, doi: 10.1007/s00170-021-07682-3.

[19] X. Liu and H. Yu, "Continuous adaptive integral-type sliding mode control based on disturbance observer for PMSM drives," *Nonlinear Dyn.*, vol. 104, no. 2, pp. 1429–1441, Apr. 2021, doi: 10.1007/s11071-021-06360-z.

[20] M. Mansouri, M. Trabelsi, H. Nounou, and M. Nounou, "Deep Learning-Based Fault Diagnosis of Photovoltaic Systems: A Comprehensive Review and Enhancement Prospects," *IEEE Access*, vol. 9, pp. 126286–126306, 2021, doi: 10.1109/ACCESS.2021.3110947.

[21] B. Yang *et al.*, "Recent Advances in Fault Diagnosis Techniques for Photovoltaic Systems: A Critical Review," *Protection and Control of Modern Power Systems*, vol. 9, no. 3, pp. 36–59, May 2024, doi: 10.23919/PCMP.2023.000583.

[22] D. U. Campos-Delgado and D. R. Espinoza-Trejo, "An Observer-Based Diagnosis Scheme for Single and Simultaneous Open-Switch Faults in Induction Motor Drives," *IEEE Transactions on Industrial Electronics*, vol. 58, no. 2, pp. 671–679, Feb. 2011, doi: 10.1109/TIE.2010.2047829.

[23] M. Salehifar, R. Salehi Arashloo, M. Moreno-Eguilaz, V. Sala, and L. Romeral, "Observer-based open transistor fault diagnosis and fault-tolerant control of five-phase permanent magnet motor drive for application in electric vehicles," *IET Power Electronics*, vol. 8, no. 1, pp. 76–87, Jan. 2015, doi: 10.1049/iet-pel.2013.0949.

[24] W.-H. Chen, J. Yang, L. Guo, and S. Li, "Disturbance-Observer-Based Control and Related Methods—An Overview," *IEEE Transactions on Industrial Electronics*, vol. 63, no. 2, pp. 1083–1095, Feb. 2016, doi: 10.1109/TIE.2015.2478397.

[25] L. Zhou, L. Cheng, C. Pan, and Z. Jiang, "Generalized Extended State Observer Based Speed Control for DC Motor Servo System," in *2018 37th Chinese Control Conference (CCC)*, IEEE, Jul. 2018, pp. 221–226. doi: 10.23919/ChiCC.2018.8483964.

[26] S. Zhuo, A. Gaillard, L. Xu, C. Liu, D. Paire, and F. Gao, "An Observer-Based Switch Open-Circuit Fault Diagnosis of DC–DC Converter for Fuel Cell Application," *IEEE Trans. Ind. Appl.*, vol. 56, no. 3, pp. 3159–3167, May 2020, doi: 10.1109/TIA.2020.2978752.

[27] J. Su, W.-H. Chen, and B. Li, "Disturbance observer based fault diagnosis," in *Proceedings of the 33rd Chinese Control Conference*, IEEE, Jul. 2014, pp. 3024–3029. doi: 10.1109/ChiCC.2014.6897123.

[28] Yaouba *et al.*, "An Experimental and Case Study on the Evaluation of the Partial Shading Impact on PV Module Performance Operating Under the Sudano-Sahelian Climate of Cameroon," *Front. Energy Res.*, vol. 10, pp. 1–13, Aug. 2022, doi: 10.3389/fenrg.2022.924285.

[29] Yaouba, A. Ayang, A. Tom, and N. Djongyang, "Adaptive Generalized Extended State Observer for a Single Phase PV Grid-connected System Operating Under the Sudanese-Sahelian Climate of Cameroon," *International Journal of Energy and Power Engineering*, vol. 13, no. 5, pp. 73–96, Nov. 2024, doi: 10.11648/j.ijepe.20241305.11.